Optical and Quantum Electronics (2021) 53:158
https://doi.org/10.1007/s11082-021-02781-7

Intensity and wavelength dependence of anisotropic nonlinear absorption inside MgO

Yinfu Zhang[1] · Tengfei Huang[1] · Liang Li[1] · Pengfei Lan[1] · Peixiang Lu[1,2]

Received: 19 October 2020 / Accepted: 30 January 2021

Abstract
We report an experimental measurement of nonlinear absorption by using the near-infrared femtosecond laser and a crystalline MgO sample. We show that the nonlinear absorption inside MgO presents a four-fold modulation as a function of the crystal alignment to the laser polarization. In different intensities and wavelengths, we observe that the modulation amplitude is changed. We introduce a model based on the calculation of the carrier density to explain the phenomenon. It shows that the varied modulation is due to the variation of effective electron mass, which is related to the crystal structure. Our work makes a step forward in the application of nonlinear absorption in exploring solid structure.

Keywords Nonlinear absorption · Modulation · The changing effective electron mass · Crystal structure

1 Introduction

Nonlinear absorption is a typical optical phenomenon between the intense laser field and the material (Kim et al. 2017; He et al. 2020; Kruchinin et al. 2018; Schiffrin et al. 2013; Wang et al. 2020; Stuart et al. 1996; Tien et al. 1999; Huang et al. 2017). It excites many nonlinear effects, such as the dynamic Franz–Keldysh effect (DFKE) (Chin et al. 2000; Jauho and Johnsen 1996), interband excitations (Schultze et al. 2014; Ernst et al. 1998), and the high-harmonic generation (HHG) in bulk solids (Ghimire et al. 2011; Vampa et al.

✉ Liang Li
liangl@hust.edu.cn

Yinfu Zhang
yinfuzhang@hust.edu.cn

Tengfei Huang
tengfeihuang@hust.edu.cn

Pengfei Lan
pengfeilan@hust.edu.cn

[1] School of Physics, Huazhong University of Science and Technology, Wuhan 430074, People's Republic of China

[2] Laboratory of Optical Information Technology, Wuhan Institute of Technology, Wuhan 430205, People's Republic of China

Published online: 06 March 2021

2015; You et al. 2017; Li et al. 2019). And it also has a widely application in laser processing technology (Weber and Nakazawa 2007; Gattass and Mazur 2008), such as laser plating and etching (Von Gutfeld et al. 1982; Simeon and Vadim 1998; Li et al. 2005). So the nonlinear absorption has become an important and active research subject in the last decades.

Since Hopfield et al. Hopfield and Worlock (1965) observed the nonlinear absorption in KI and CsI, many studies of nonlinear absorption in solids had been reported both experimentally and theoretically (Rayner et al. 2005; Gertsvolf et al. 2008; Rajeev et al. 2009; Li et al. 2020; Hollinger et al. 2019; Grojo et al. 2013; Dachraoui et al. 2011; Temnov et al. 2006; Ghimire et al. 2011; Kirkwood et al. 2011). Rayner et al. reported the nonlinear absorption in the Pyrex sample and introduced a self-limiting absorption model to fit the experiment (Rayner et al. 2005). According to their work, nonlinear absorption happens once the intensity exceeds a threshold. By using the self-limiting absorption model, Gertsvolf *et al.* explained the modulation of nonlinear absorption in several wide-bandgap crystals (Gertsvolf et al. 2008). They found that the modulation could be attributed to the orientation dependence of the effective electron mass. Another study observed a similar modulation in a LiF crystal (Dachraoui et al. 2011). They found that the nonlinear absorption is at its maximum when the laser polarization is parallel to $\Gamma - M$ and at its minimum when the laser field is along $\Gamma - K$. It implies that the nonlinear absorption can be a structural probe in solids. To get the solids structure from the nonlinear absorption, one needs to reveal the quantitative relation of them. In recent years, Kirkwood et al. discussed a way to model the modulation of the nonlinear absorption (Kirkwood et al. 2011). It is based on the effective electron mass estimated from band gap calculations using density functional theory (DFT). However, the method has not been tested to reproduce the experimental modulation. Furthermore, inspired by the anisotropic investigation of MgO, which reported the relation between HHG and the solid structure (You et al. 2017), we report the effect of structures on the nonlinear absorption. By studying the nonlinear absorption of MgO, we present another perspective of the study on crystal structures.

In this paper, we report the nonlinear absorption inside a MgO crystal by using a near-infrared femtosecond laser. We observe that the nonlinear absorption presents a modulation as a function of the crystal alignment to the laser polarization direction. By controlling the strength and the wavelengths of laser fields, we find that the modulation is varied. To explain the variation of the nonlinear absorption, we improve the model based on the calculation of the carrier generation (Rajeev et al. 2009; Li et al. 2020). Using the modified model, we calculate the nonlinear absorption. The result is in good agreement with the experiment.

2 Experimental methods

Figure 1 shows the schematic diagram of the experiment setup. In our experiment, a femtosecond laser pulse (55 fs, 1300 nm) is focused onto a 001-cut MgO crystal, which is synthesized by electric arc process. The crystal is 200-μm-thick, and its size is 1×1 cm^2. To explore the effect of wavelengths, we make a similar measurement using a 45-fs, 800-nm laser pulse. The 800-nm laser pulse is obtained from an amplified Ti:sapphire laser system, which produces 7 mJ per pulse at a repetition rate of 1 kHz (Zhai et al. 2020; Shao et al. 2020). The 1300-nm laser is generated from a two-stage optical parametric amplification (OPA) pumped by the 800-nm pulse. The pulse duration is measured by a home-built

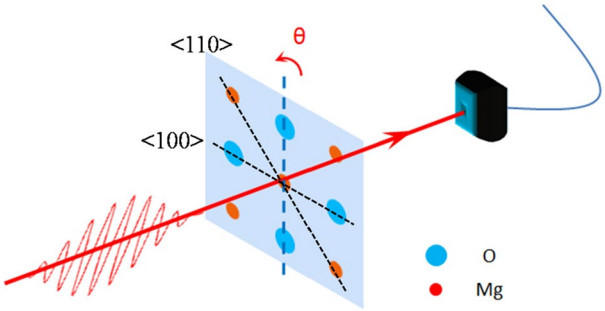

Fig. 1 Schematic diagram of the optical setup of the transmission measurement. An intense linear femtosecond laser pulse is focused into the 200-μm-thick, 001-cut MgO crystal. The crystal is rotated to various angles alignment (θ) to the fixed laser polarization. The laser propagates along the crystallographic axis, ⟨001⟩. The dashed blue line is shown as the laser polarization. The Mg–Mg (⟨110⟩) and Mg–O direction (⟨100⟩) are indicated as dashed black lines. The transmission signal is collected by a photodiode. (Color figure online)

autocorrelator. The polarization is linear, and the intensity is varied from 4 TW/cm^2 to 36 TW/cm^2 (below the threshold of self-focusing) by rotating a half-wave plate (HWP) before a polarizer. We use a f = 10 cm CaF_2 lens to focus the pulse. The spot size is about 20 μm in vacuum. The MgO sample is fixed on a motor-driven translation stage to keep every pulse focusing on a new spot by moving it (Rajeev et al. 2006). For controlling the lattice alignment relative to the laser polarization, MgO is mounted in a rotating mount. The sample is rotated around the axis given by laser propagation (the crystallographic axis, ⟨001⟩). We obtain the nonlinear absorption in MgO by measuring the laser pulse transmission passing through the crystal. The transmission signal is collimated by a CaF_2 lens (f = 10 cm) and collected by a photodiode connected with a computer. All the transmission signal is normalized by the transmission (T_0) measured when the crystal is moved away from the focus to eliminate the influence of air/material interface reflections (Bahae et al. 1990; Leyder et al. 2013). The raw data are five-points average.

3 Theoretical methods

Nonlinear absorption in solid is related to the generation of carriers. In our work, the production of carriers is given by the contribution of multiphoton ionization and avalanche ionization. So the carrier generation rate is expressed by Rayner et al. (2005), Rajeev et al. (2009), Dachraoui et al. (2011)

$$\frac{dn}{dt} = W(I) + \alpha In, \tag{1}$$

where n is the carrier density, α is the avalanche coefficient. The first term on the right-hand side of Eq. (1) is the multiphoton ionization rate, which is given by

$$W(I) = \sigma_k I^k \tag{2}$$

where k is the multiphoton ionization order. σ_k is the multiphoton ionization cross section described by Dachraoui et al. (2011), Keldysh (1958, 1965)

$$\sigma_k = \frac{2\omega}{9\pi}\left(\frac{m^*\omega}{\hbar}\right)^{3/2}\phi\left(\sqrt{2k-\left(\frac{2}{\hbar\omega}\left(E_g+\frac{e^2E_L^2}{em^*\omega}\right)\right)}\right) \times \exp\left\{2k\left(1-\frac{1}{4\gamma^2}\right)\right\}\left(\frac{1}{16\gamma^2}\right)^k, \tag{3}$$

where the function ϕ denotes Dawson's integral, defined by $\phi(z) = \int_0^z e^{t^2-z^2}dt$, E_g is the bandgap of solids (E_g=7.8 eV), E_L and ω is the amplitude and the frequency of the laser, and γ is the Keldysh parameter (Keldysh 1965), which is given by

$$\gamma = \frac{\omega\sqrt{m^*Eg}}{eE_L}, \tag{4}$$

The second term on the right is the rate of avalanche ionization. Under the flux-doubling approximation, the avalanche coefficient is given by Ridley (2013)

$$\alpha = \frac{2p}{\varepsilon_0 c\int_0^{U_p} 1/\kappa(\varepsilon)d\varepsilon}, \tag{5}$$

where p is constant, whose value is between 0.5 and 1, c is the velocity of light, U_p is the electron energy threshold for collisional ionization (about 1.42 E_g in MgO Ridley 2013), and κ is the conductivity per electron at electron energy ε, given by

$$\kappa = \frac{e^2}{m^*}\frac{\tau_c(\varepsilon)}{[1+\tau_c(\varepsilon)^2\omega^2]}, \tag{6}$$

Here $1/\tau_c(\varepsilon)$ is the electron-phonon momentum collision rate. For $\tau_c(\varepsilon)$ independent of ε, and with $p = 1$, the coefficient is simplified by Rajeev et al. (2009)

$$\alpha = \frac{2\kappa}{\varepsilon_0 c U_p}, \tag{7}$$

In Eqs.(3–4) and (6), m^* is the effective electron mass. According to the band theory, we get the expression of m^* :

$$\left(\frac{1}{m^*}\right)_{ij} = \frac{1}{\hbar^2}\cdot\frac{\partial^2 E}{\partial k_i \partial k_j} \quad i,j = x,y \tag{8}$$

where E is the energy band dispersion equation, which can be obtained from the first principles based on DFT (Kresse and Furthmuller 1996a, b; Perdew et al. 1996; Zhao et al. 2019).

4 Results and discussions

In this paper, we measure the transmitted laser energy to obtain the experimental data of the nonlinear absorption, which is given by subtracting the transmission from the total energy. In Fig. 2a, the transmission is measured in MgO as a function of the crystal alignment to the 1300-nm laser polarization. The intensity is 17 TW/cm^2, 27 TW/cm^2 and 33 TW/cm^2. The transmission is at its minimum when the laser polarization is along θ=0°,

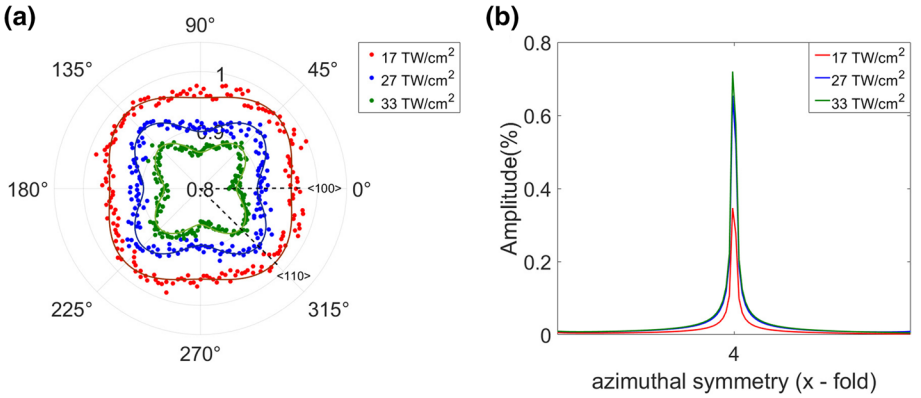

Fig. 2 **a** Transmission measured in a 001-cut MgO as a function of the alignment of the laser polarization to the crystal lattice in different intensities. The wavelength of laser is 1300 nm. The points are the experimental measurements and the solid lines are the modulation profiles. The Mg–O (⟨100⟩) and Mg–Mg directions (⟨110⟩) are indicated as dashed black lines. **b** Transmission modulation spectra for the experiments in (**a**). The amplitude is normalized by the component of zero-fold frequency

90°, 180°, and 270°, which correspond to the Mg–O directions (⟨100⟩, shown in Fig. 1). The transmission is at its maximum with θ=45°, 135°, 225°, and 315° corresponding to the Mg–Mg (or O–O) directions (⟨110⟩, shown in Fig. 1). It shows a modulation with a $\pi/2$ rotational period in different intensities. With the laser field increasing, the modulation is more distinct. To show the modulation clearly, we apply a discrete Fourier transform. The signal modulation frequency spectra are shown in Fig. 2b. The abscissa is the recurrence frequency of the alignment angle. The ordinate is the amplitude of modulation, which is normalized by the zero-frequency component. For excluding the noise, we make an inverse Fourier transform, considering only components of zero and four-fold frequency. The results are shown as solid lines in Fig. 2a. They are in good agreement with the experiment data. So the other frequency components (not shown in the figure) caused by noise have little contribution to the modulation. In the comparison of the modulation amplitude, we observe that the amplitude increases with the intensity increasing.

We also make a similar measurement of nonlinear absorption in different wavelengths. Setting the intensity at 27 TW/cm^2, the transmission in 800 nm and 1300 nm is shown in Fig. 3. We apply the same method, discrete Fourier transform, to examine the modulation. A four-fold symmetry is seen on the transmission in both wavelengths. The modulation amplitude in 800 nm is higher than that in 1300 nm. It indicates that the wavelength of the laser also influences the nonlinear absorption.

From these observations in Figs. 2 and 3, we find that nonlinear absorption is orientation dependent. The modulation depth is related to the strength and wavelength of the laser field. To explain the varied modulation depth, we discuss the nonlinear absorption using the model described in Sect. 3.

To explore the relation of the laser field and the modulation, we measure the transmission rate of the 1300-nm laser pulse as a function of the intensity along θ=0°, 45°. As shown in Fig. 5, the blue dots are the transmission data along 0°, and the red dots are the transmission data along 45°. We observe that the difference of transmission between the two alignments enlarges when the laser field strengthens. It corresponds to a deeper modulation at a stronger laser field as shown in Fig. 2.

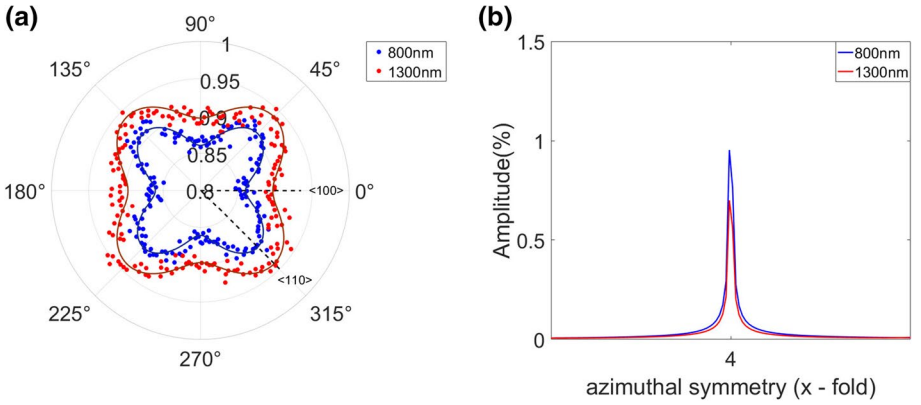

Fig. 3 **a** Transmission measured in a 001-cut MgO crystal in different wavelengths. The intensity is fixed at 27 TW/cm^2. The Mg–O ($\langle 100 \rangle$) and Mg–Mg directions ($\langle 110 \rangle$) are indicated as dashed black lines. **b** Transmission modulation spectra for the experiment data in (**a**)

Then we fit the experimental transmission by numerical analysis. According to Eq. (1), we get the carrier generation rate from two parts, multiphoton ionization and avalanche ionization. As shown in Eqs.(3) and (7), these two parts are influenced by the effective electron mass related to the solid structure. According to the band theory, we obtain the two-dimensional band structure (Huang et al. 2017; Wu et al. 2015). Based on Eq. (8), we get the effective electron mass along different alignments shown with a color bar in reciprocal space in Fig. 6. The value is defined as m^*/m_e, where m_e is the rest mass of electron.

In Rajeev et al. (2009), Rajeev et al. approximated the multiphoton ionization rate with a fixed cross section in different intensities. According to Eq. (3), we obtain the cross section by using a fixed value of the effective electron mass. Then we use the cross section to calculate the multiphoton ionization term of the nonlinear absorption based on Eq. (2). By inserting Eq. (2) into Eq. (1), the calculations of the transmission are shown as dashed lines in Fig. 5. The transmission is defined by $T = (E_{pulse} - nE_g)/E_{pulse}$, where E_{pulse} is the total energy of the laser pulse. The dashed bule line is the result along 0°, and the dashed red line is that along 45°. At the low field strength (below 23 TW/cm^2), the calculations agree with the experiments well. But at the relative high field strength, there is a deviation between the experiments and the calculations. In our experimental conditions, the multiphoton ionization dominants the nonlinear absorption (Stuart et al. 1996; Tien et al. 1999). So we need to modify the multiphoton ionization term in the model of the carrier generation rate.

Considering the effect of the laser field, we apply a changing value of the effective electron mass to calculate the carrier density. In Fig. 6, we obtain the distribution of the effective electron mass in reciprocal space according to Eq. (8). In the laser field, the electrons oscillate in the valence band and transform into the conduction band with different initial momenta. With the initial momenta of electrons increasing, the effective electron mass is larger, and the gap is wider between the valence band and the conduction band. The multiphoton ionization is contributed by several channels (Li et al. 2019). So that Eq. (2) can be modified by

$$W(I) = c_1\sigma_k I^k + c_2\sigma_{k+1} I^{k+1} + c_3\sigma_{k+2} I^{k+2} + \cdots \tag{9}$$

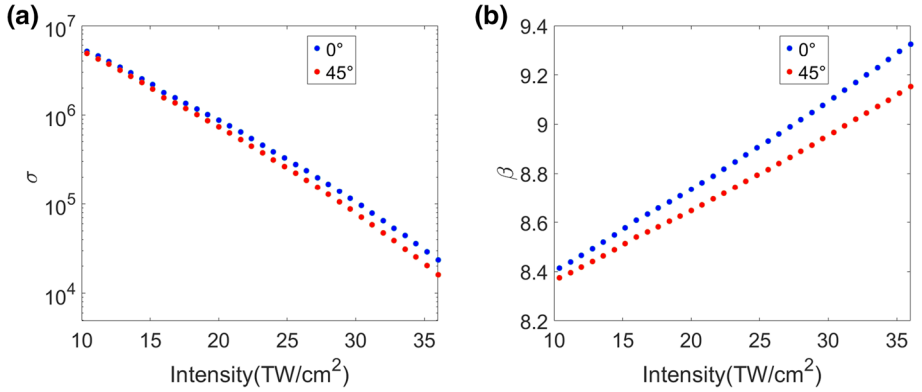

Fig. 4 The dependences of σ and β on laser field. **a** The cross-section of the multiphoton ionization as a function of the intensity. The blue dots are values along the Mg–O directions (0°, ⟨100⟩) and the red dots are values along the Mg–Mg direction (45°, ⟨110⟩). The unit of σ is not fixed, described as (TW cm^{-2})$^{-\beta}$ cm^{-3}ps^{-1}. **b** The dependence of multiphoton ionization order on the intensity. The blue dots are values along the Mg–O directions (0°, ⟨100⟩) and the red dots are values along the Mg–Mg direction (45°, ⟨110⟩). (Color figure online)

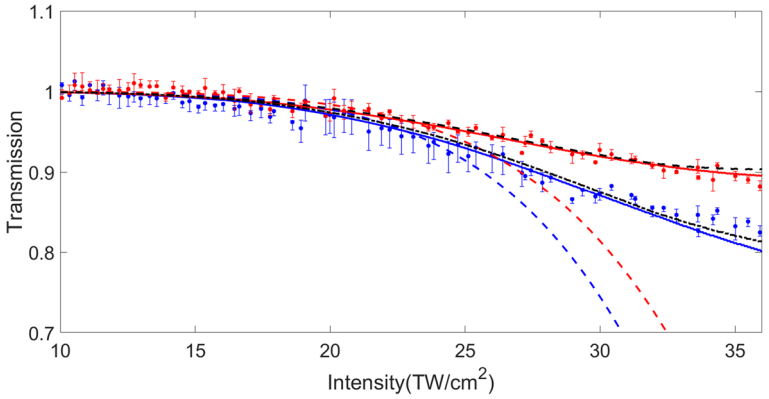

Fig. 5 Numerical fits to the transmission as a function of the 1300-nm laser field strength along 0° and 45°. The points are the experimental measurements. The dashed blue lines and dashed red lines are the result of the model using the Eq. (1), where k is set at 8 in the multiphoton ionization term. The solid lines are obtained by using Eq. (10) to calculate the multiphoton ionization term. The blue are the results along 0° (Γ-X direction), and the red are the results along 45° (Γ-K direction). The dashed black lines show the domination of multiphoton ionization on the nonlinear absorption. (Color figure online)

where k is the multiphoton ionization order. c_1, c_2, c_3 are the coefficients, which are changeable in different intensities. Eq. (9) can be simplified to

$$W(I) \approx \sigma(I) I^{\beta(I)} \tag{10}$$

where $\sigma(I)$ is the cross-section and $\beta(I)$ is the multiphoton ionization order. They are dependent on the field strength because of the changing effective electron mass. The dependences of σ and β on the laser field are shown in Fig. 4. The blue dots are values along 0°, and the red are values along 45°.

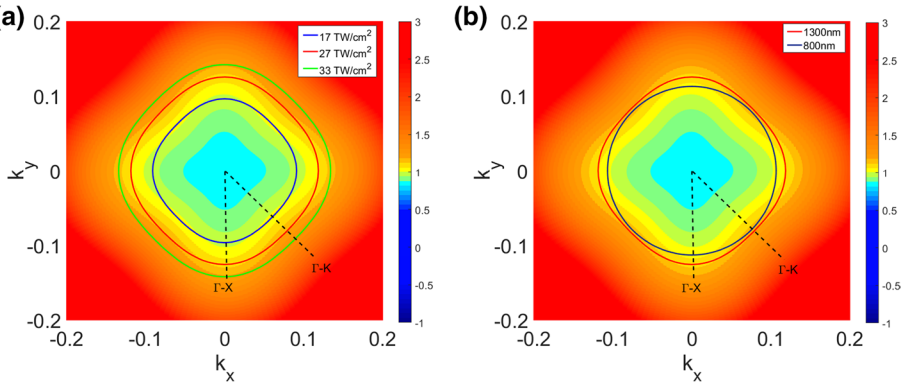

Fig. 6 The distribution of the effective electron mass along the polarization of laser field in reciprocal space. The value is defined as m^*/m_e, where m_e is the rest mass of electron. The dashed black lines indicate Γ-X (0°, 90°, 180° and 270°, ⟨100⟩) and Γ-K direction (45°, 135°, 225° and 315°, ⟨110⟩). **a** The solid lines are the distribution of the effective electron mass used in our model in three different intensities. **b** The solid lines are the distribution of the effective electron mass used in our model at two wavelengths

We obtain the calculated transmission curves (the solid lines as shown in Fig. 5) by using Eq. (10) to calculate the multiphoton ionization term. We can see that the calculations fit the experimental data well. It shows that the effective electron mass is changed when the intensity increases. In the moderate intense laser field, more electrons are ionized to conduction band by higher order channels. So that the nonlinear absorption is not as big as the calculation shown as the dashed lines. In addition, the dashed black lines in Fig. 5 present the contribution of multiphoton ionization on nonlinear absorption. They show the domination of the multiphoton process, which is consistent with the previous work (Stuart et al. 1996; Tien et al. 1999).

Setting the intensity at 17 TW/cm^2, 27 TW/cm^2, and 33 TW/cm^2, we show the distribution of the effective electron mass in reciprocal space as solid lines in Fig. 6a. We can observe that the effective electron mass changes along different alignments at a fixed field strength. The mass is at its maximum along the Γ-K direction (45°, 135°, 225°, 315°), and at its minimum along the Γ-X direction (0°, 90°, 180°, 270°). When the laser field strengthens, the initial momenta of electrons increase, and the effective electron mass rises. The variation of the mass depends on the alignment. In Fig. 7, we show the effective electron mass as a function of intensity in reciprocal space along two specific directions, the Γ-X direction (the solid blue line) and the Γ-K direction (the solid red line). Along the Γ-K direction, the effective electron mass are larger than that along the Γ-X direction. With the intensity increasing, the difference of the effective electron mass is enlarged along the two directions. It causes a larger modulation amplitude in a higher laser field, as shown in Fig. 2.

Besides, we reproduce the modulation based on the calculation of the nonlinear absorption. By considering the calculated effective electron mass, we obtain the transmission along different alignments in the 1300-nm laser field at a strength of 27 TW/cm^2. The result is shown in Fig. 8. The red dots are the experimental data, and the solid blue line is the calculation. They are in good agreement. It indicates that the four-fold modulation of nonlinear absorption is due to the orientation dependence of the effective electron mass.

The wavelength also affects the effective electron mass, as shown in Fig. 6b. The effective electron mass in the 1300-nm laser field is larger than that in the 800-nm laser field. Along

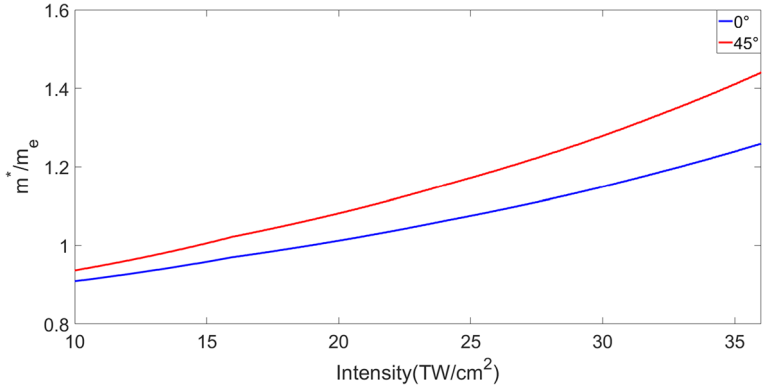

Fig. 7 Comparison of the effective electron mass used in the Eq. (10) in reciprocal space as a function of the intensity. The ordinate is defined as m^*/m_e. The blue line is the effective electron mass along the Γ-X direction (0°), and the red line is the effective electron mass along the Γ-K direction (45°). (Color figure online)

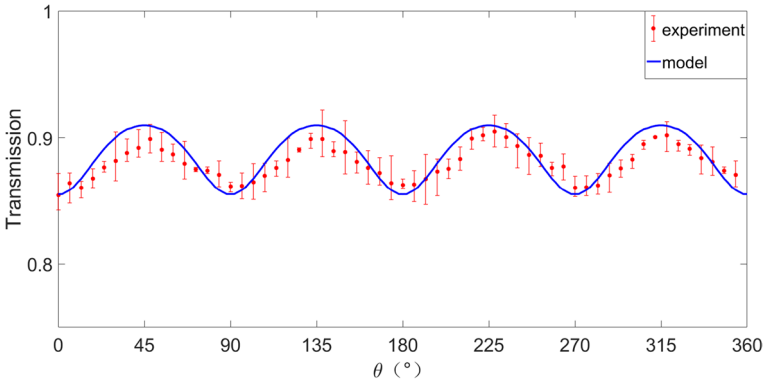

Fig. 8 The fitting result of the anisotropic transmission between experiments and calculations in 1300 nm at a strength of 27 TW/cm^2. The red dots are the transmission data measured as a function of the angle of MgO crystal alignment to the laser polarization. The blue solid line is the calculation using the model based on the generation rate of carrier density. (Color figure online)

the Γ-K directions, the effective electron mass is similar. But along the Γ-X directions, the effective electron mass is smaller in the 800-nm field. Therefore the difference of the effective electron mass along the two directions is larger in the 800-nm laser field. It results in a larger modulation amplitude than in 1300 nm, as shown in Fig. 3. To show the solid structure clearly, it is necessary to choose an appropriate wavelength to obtain a distinct modulation of the nonlinear absorption.

5 Conclusion

In summary, we report measurements of the nonlinear absorption on the alignment of MgO crystal to the laser polarization in different intensities and wavelengths. We observe that the nonlinear absorption has a four-fold modulation, and the depth of the modulation is varied by changing the intensity and the wavelength. Using a model based on the calculation of the generation rate of carrier density, we reproduce the modulation of the nonlinear absorption. We find that the varied modulation is due to the changing of the effective electron mass in different intensities and wavelengths. By this work, we further reveal the relation of the nonlinear absorption and the effective electron mass. Considering that the mass is related to the energy band structure, we show the potential application of the nonlinear absorption on exploring the crystal structures.

Acknowledgements This paper is supported by National Natural Science Foundation of China (91950202, 11627809, 11874165, 11704137, 11774109, 11904192).

References

Bahae, M.S., Said, A.A., Wei, T.H., Hagan, D.J., Van Stryland, E.W.: Sensitive measurement of optical nonlinearities using a single beam. IEEE J. Quantum Electron. **26**, 4 (1990)

Chin, A.H., Bakker, J.M., Kono, J.: Ultrafast electroabsorption at the transition between classical and quantum response. Phys. Rev. Lett. **85**, 3293–3296 (2000)

Dachraoui, H., Oberer, C., Heinzmann, U.: Femtosecond crystallographic experiment in wide-bandgap LiF crystal. Opt. Express **19**(3), 2797–2804 (2011)

Ernst, H.J., Charra, F., Douillard, L.: Interband electronic excitation-assisted atomic-scale restructuring of metal surfaces by nanosecond pulsed laser light. Science **279**(5351), 679–681 (1998)

Gattass, R.R., Mazur, E.: Femtosecond laser micromachining in transparent materials. Nat. Photon. **2**, 219–225 (2008)

Gertsvolf, M., Jean-Ruel, H., Rajeev, P.P., Klug, D.D., Rayner, D.M., Corkum, P.B.: Orientation-dependent multiphoton ionization in wide band gap crystals. Phys. Rev. Lett. **101**, 243001 (2008)

Ghimire, S., DiChiara, A.D., Sistrunk, E., Agostini, P., DiMauro, L.F., Reis, D.A.: Observation of high-order harmonic generation in a bulk crystal. Nat. Phys. **7**, 138–141 (2011)

Ghimire, S., DiChiara, A.D., Sistrunk, E., Szafruga, U.B., Agostini, P., DiMauro, L.F., Reis, D.A.: Redshift in the optical absorption of ZnO single crystals in the presence of an intense midinfrared laser field. Phys. Rev. Lett. **107**, 167407 (2011)

Grojo, D., Leyder, S., Delaporte, P., Marine, W., Sentis, M., Utéza, O.: Long-wavelength multiphoton ionization inside band-gap solids. Phys. Rev. B **88**, 195135 (2013)

Von Gutfeld, R.J., Romankiw, L.T., Acosta, R.E.: Laser-enhanced plating and etching: mechanisms and applications. IBM **26**(2), 136–144 (1982)

He, Y., He, L., Wang, P., Wang, B., Sun, S., Liu, R., Wang, B., Lan, P., Lu, P.: Measuring the rotational temperature and pump intensity in molecular alignment experiments via high harmonic generation. Opt. Express **28**(14), 21182–21191 (2020)

Hollinger, R., Gupta, D., Zapf, M., Karst, M., Röder, R., Uschmann, I., Reislöhner, U., Kartashov, D., Ronning, C., Spielmann, C.: Polarization dependent multiphoton absorption in ZnO thin films. J. Phys. D **53**, 055102 (2019)

Hopfield, J.J., Worlock, J.M.: Two-quantum absorption spectrum of KI and CsI. Phys. Rev. **137**, A1455–1464 (1965)

Huang, T., Zhu, X., Li, L., Liu, X., Lan, P., Lu, P.: High-order-harmonic generation of a doped semiconductor. Phys. Rev. A **96**, 043425 (2017)

Jauho, A.P., Johnsen, K.: Dynamical Franz–Keldysh effect. Phys. Rev. Lett. **76**(24), 4576–4579 (1996)

Keldysh, L.V.: Behavior of non-metallic crystals in strong electric fields. Sov. Phys. JETP **6**, 763–770 (1958)

Keldysh, L.V.: Ionization in the field of a strong electromagnetic wave. Sov. Phys. JETP **20**, 1307–1314 (1965)
Kim, H., Han, S., Kim, Y.W., Kim, S., Kim, S.W.: Generation of coherent extreme-ultraviolet radiation from bulk sapphire crystal. ACS Photon. **4**, 1627–1632 (2017)
Kirkwood, D.A., Golin, S., Chalus, O., Thai, A., Biegert, J., Klug, D.D., Rayner, D.M., Corkum, P.B.: Crystal structure measured by nonlinear absorption using 3.1 um femtosecond laser pulses. In: CLEO-laser applications to photonic applications (2011)
Kresse, G., Furthmuller, J.: Efficient iterative schemes for ab initio total-energy calculations using a plane-wave basis set. Phys. Rev. B **54**, 11169–11186 (1996a)
Kresse, G., Furthmuller, J.: Efficiency of ab-initio total energy calculations for metals and semiconductors using a plane-wave basis set. Comput. Mater. Sci. **6**, 15–50 (1996b)
Kruchinin, S.Y., Krausz, F., Yakovlev, V.S.: Colloquium: strong-field phenomena in periodic systems. Rev. Mod. Phys. **90**, 021002 (2018)
Leyder, S., Grojo, D., Delaporte, P., Lebugle, M., Marine, W., Sanner, N., Sentis, M., Utéza, O.: On the wavelength dependence of femtosecond laser interactions inside band gap solids. In: Proceedings of the SPIE, vol. 8611 (2013)
Li, C., Feng, D., Jia, T., Sun, H., Li, X., Xu, S., Wang, X., Xu, Z.: Ultrafast dynamics in ZnO thin films irradiated by femtosecond lasers. Solid State Commun. **136**, 389–394 (2005)
Li, L., Lan, P., He, L., Cao, W., Zhang, Q., Lu, P.: Determination of electron band structure using temporal interferometry. Phys. Rev. Lett. **124**, 157403 (2020)
Li, L., Lan, P., Zhu, X., Huang, T., Zhang, Q., Manfred, L., Lu, P.: Reciprocal-space-trajectory perspective on high-harmonic generation in solids. Phys. Rev. Lett. **122**, 193901 (2019)
Li, J., Li, L., Zhang, Q., Zhu, X., Huang, T., Lan, P., Lu, P.: Channel-closing effects of electronic excitation in solids. Opt. Express **27**(26), 37224–37235 (2019)
Perdew, J.P., Burke, K., Ernzerhof, M.: Generalized gradient approximation made simple. Phys. Rev. Lett. **77**, 3865–3868 (1996)
Rajeev, P.P., Gertsvolf, M., Corkum, P.B., Rayner, D.M.: Field dependent avalanche ionization rates in dielectrics. Phys. Rev. Lett. **102**, 083001 (2009)
Rajeev, P.P., Gertsvolf, M., Simova, E., Hnatovsky, C., Taylor, R.S., Bhardwaj, V.R., Rayner, D.M., Corkum, P.B.: Memory in nonlinear ionization of transparent solids. Phys. Rev. Lett. **97**, 253001 (2006)
Rayner, D.M., Naumov, A., Corkum, P.B.: Ultrashort pulse non-linear optical absorption in transparent media. Opt. Express **13**, 3208–3217 (2005)
Ridley B.K.: Quantum Processes in Semiconductors. Oxford University Press, Oxford (2013)
Schiffrin, A., Paasch-Colberg, T., Karpowicz, N., Apalkov, V., Gerster, D., Muhlbrandt, S., Korbman, M., Reichert, J., Schultze, M., Holzner, S., Barth, J.V., Kienberger, R., Ernstorfer, R., Yakovlev, V.S., Stockman, M.I., Krausz, F.: Optical-field-induced current in dielectrics. Nature **493**(7430), 70–74 (2013)
Schultze, M., Ramasesha, K., Pemmaraju, C.D., Sato, S.A., Whitmore, D., Gandman, A., Prell, J.S., Borja, L.J., Prendergast, D., Yabana, K., Neumark, D.M., Leone, S.R.: Attosecond band-gap dynamics in silicon. Science **346**, 6215 (2014)
Shao, R., Zhai, C., Zhang, Y., Sun, N., Cao, W., Lan, P., Lu, P.: Generation of isolated circularly polarized attosecond pulses by three-color laser field mixing. Opt. Express **28**, 15874–15884 (2020)
Simeon, M.M., Vadim, P.V.: Laser-assisted microtechnology. Springer, Berlin, Heidelberg (1998)
Stuart, B.C., Feit, M.D., Herman, S., Rubenchik, A.M., Shore, B.W., Perry, M.D.: Nanosecond-to-femtosecond laser-induced breakdown in dielectrics. Phys. Rev. B **53**(4), 1749–1761 (1996)
Temnov, V.V., Sokolowski-Tinten, K., Zhou, P., El-Khamhawy, A., von der Linde, D.: Multiphoton ionization in dielectrics: comparison of circular and linear polarization. Phys. Rev. Lett. **97**, 237403 (2006)
Tien, A.C., Backus, S., Kapteyn, H., Murnane, M., Mourou, G.: Short-pulse laser damage in transparent materials as a function of pulse duration. Phys. Rev. Lett. **82**(19), 3883–3886 (1999)
Vampa, G., McDonald, C.R., Orlando, G., Corkum, P.B., Brabec, T.: Semiclassical analysis of high harmonic generation in bulk crystals. Phys. Rev. B **91**(6), 064302 (2015)
Wang, D., Zhu, X., Yuan, H., Lan, P., Lu, P.: Interference effect in high-order harmonic generation from degenerate current-carrying orbitals of polyatomic molecules. Phys. Rev. A **101**, 023406 (2020)
Weber, H.G., Nakazawa, M.: Ultrahigh-speed optical transmission technology. Springer, New York (2007)
Wu, M., Ghimire, S., Reis, D.A., Schafer, K.J., Gaarde, M.B.: High-harmonic generation from bloch electrons in solids. Phys. Rev. A **91**(4), 043839 (2015)

You, Y.S., Reis, D.A., Ghimire, S.: Anisotropic high-harmonic generation in bulk crystals. Nat. Phys. **13**, 345–350 (2017)

Zhai, C., Shao, R., Lan, P., Wang, B., Zhang, Y., Yuan, H., Njoroge, S.M., He, L., Lu, P.: Ellipticity control of high-order harmonic generation with nearly orthogonal two-color laser fields. Phys. Rev. A **101**, 053407 (2020)

Zhao, Y., Ma, S., Jiang, S., Yang, Y., Zhao, X., Chen, J.: All-optical reconstruction of k-dependent transition dipole moment by solid harmonic spectra from ultrashort laser pulses. Opt. Express **27**, 34392–34404 (2019)